The Effect of Galactic Aberration on the CRF

David Mayer [1], Sébastien Lambert [2], Johannes Böhm [1], Hana Krásná [1,3], Niu Liu [2,4]

Abstract We compare two Celestial Reference Frame (CRF) solutions made from Very Long Baseline Interferometry (VLBI) group delay observations in S/X band using vector spherical harmonics. In both solutions the same data set was used which consists of almost all observations since 1979 until the beginning of 2018. The same parameterization and models were used with the exception that in one of the solutions the effect of galactic aberration (GA) was corrected. The other solution serves as a reference. We show that the deformation of a CRF estimated with the whole set of VLBI observations can be described by a systematic dipole displacement with an amplitude of about 35 μas.

Keywords CRF, Galacto-centric acceleration, vector spherical harmonics

1 Introduction

The solar system is rotating around the galactic center. This introduces a galacto-centric acceleration, which, in turn, imprints itself as an apparent proper motion of celestial objects. The term galactic aberration (GA) is used for this effect. On the one hand, this is a problem for Very Long Baseline Interferometry (VLBI), since the sources are assumed stationary, which should be corrected. On the other hand, since quasars are very stable reference objects, which do not have detectable proper motions, we can use VLBI to assess this phenomenon. Several papers were published with the aim of estimating GA from Very Long Baseline Interferometry (VLBI) data (see, e.g., [12, 16, 13, 14]). They report values ranging from 5.2 ± 0.2 to 6.4 ± 1.1 with the center of the Galaxy at $17^{\mathrm{h}}45^{\mathrm{m}}40^{\mathrm{s}}$ in right ascension and $-29°00'28''$ in declination. The International VLBI Service for Geodesy and Astrometry (IVS) initiated a working group, which was tasked with the investigation of this effect. At the IVS General Meeting in 2018, the working group presented their recommendations. The GA was estimated with 5.6 μas per year and it was recommended to remove this effect at the modeling stage, see [9]. However, for consistency reasons this value was recalculated using the data set, which was used for the calculations of the International Celestial Reference Frame 3 (ICRF3), see [4]. The fully consistent (with ICRF3) estimate of GA was found to be 5.8 μas per year. The ICRF3, which is the newly recommended international celestial reference frame, utilizes this value to model the effect of GA. In order to correct a time dependent effect an epoch has to be chosen. The average mean epoch of sources in S/X band published in ICRF3 is December 2012 and the epoch for which GA is corrected is 2015. The same value of 5.8 μas per year with the same epoch of 2015 was used in the CRF solution evaluated here. We can expect that the correction of GA has some systematic effect on the celestial reference frame. This systematic is imprinted onto the difference vectors between two solutions, one where GA was corrected and one where it was not.

In order to quantify this effect the method of vector spherical harmonics, see [10], is used. Global features of the differences such as a rotation of the catalogs and the so-called glide parameters are reflected in degree 1. Degree 2 describes the quadrupole deformations between the catalogs. The whole transformation reads:

1. Technische Universität Wien, Austria
2. Observatoire de Paris, France,
3. Czech Academy of Sciences, Czech Republic
4. School of Astronomy & Space Science, China

$$
\begin{aligned}
\Delta\alpha\cos\delta &= R_1\cos\alpha\sin\delta + R_2\sin\alpha\sin\delta - R_3\cos\delta \\
&\quad - D_1\sin\alpha + D_2\cos\alpha \\
&\quad + a_{20}^{M}\sin 2\delta \\
&\quad + \left(a_{21}^{E,\mathrm{Re}}\sin\alpha + a_{21}^{E,\mathrm{Im}}\cos\alpha\right)\sin\delta \qquad (1)\\
&\quad - \left(a_{21}^{M,\mathrm{Re}}\cos\alpha - a_{21}^{M,\mathrm{Im}}\sin\alpha\right)\cos 2\delta \\
&\quad - 2\left(a_{22}^{E,\mathrm{Re}}\sin 2\alpha + a_{22}^{E,\mathrm{Im}}\cos 2\alpha\right)\cos\delta \\
&\quad - \left(a_{22}^{M,\mathrm{Re}}\cos 2\alpha - a_{22}^{M,\mathrm{Im}}\sin 2\alpha\right)\sin 2\delta, \\
\Delta\delta &= -R_1\sin\alpha + R_2\cos\alpha \\
&\quad - D_1\cos\alpha\sin\delta - D_2\sin\alpha\sin\delta + D_3\cos\delta \\
&\quad + a_{20}^{E}\sin 2\delta \\
&\quad - \left(a_{21}^{E,\mathrm{Re}}\cos\alpha - a_{21}^{E,\mathrm{Im}}\sin\alpha\right)\cos 2\delta \qquad (2)\\
&\quad - \left(a_{21}^{M,\mathrm{Re}}\sin\alpha + a_{21}^{M,\mathrm{Im}}\cos\alpha\right)\sin\delta \\
&\quad - \left(a_{22}^{E,\mathrm{Re}}\cos 2\alpha - a_{22}^{E,\mathrm{Im}}\sin 2\alpha\right)\sin 2\delta \\
&\quad + 2\left(a_{22}^{M,\mathrm{Re}}\sin 2\alpha + a_{22}^{M,\mathrm{Im}}\cos 2\alpha\right)\cos\delta
\end{aligned}
$$

where R_i are the three rotation parameters, D_i are the three glide parameters, and $a_{lm}^{M,E}$ are the quadrupole parameters of electric (E) and magnetic (M) type.

2 Data

The data used for this comparison is equivalent to the data set used for the S/X band solution within ICRF3. It spans almost 40 years from 1979 until the beginning of 2018 with 6,000 observing sessions. More than 100 stations collected about 12 million group delay observations from more than 4,500 sources.

3 Analysis

Two celestial reference frames were estimated with the software VieVS [3]. Single sessions were analyzed first and the normal equation system from each session was saved. The normal equation systems were then stacked in a following global solution, which results in a global celestial and terrestrial reference frame.

Generally, the IERS 2010 Conventions [11] were used for a priori modeling. The following provides a short overview of parameters that were used in the single session analysis:

- ITRF2014 (see [1]) and ICRF2 (see [5] and [6]) were used as a priori Terrestrial Reference Frame (TRF) and CRF, respectively.
- The Vienna Mapping Function (VMF1), see [2], was used as mapping function, the DAO model was used for a priori gradients, see [7] and [8], and the atmospheric pressure loading (APLO) model by [15] was used.
- Clocks were estimated as quadratic functions with piece wise linear offsets (PWLO) every hour.
- Troposphere delays were estimated as zenith wet delays and north/east gradients every 30 min and six hours, respectively. Absolute constraints were used for the gradients in order to prevent unrealistic values.
- Earth orientation parameters (EOP) were estimated every 48h with tight relative constraints between these offsets, effectively constraining them to a single offset.
- Sources, which have less than three observations, were excluded at the observation level.

In the global solution, the following parameters were used:

- Stations with a short observing history were reduced, which means that their position was estimated session-wise.
- Known breaks from earthquakes and other sources were introduced.
- Velocity constraints for stations at the same site are introduced.
- Station positions and velocities are estimated, the datum is set to 21 well-behaved stations.
- The special handling sources were reduced. Note that this is different in the ICRF3 solution where all sources are estimated as global parameters.
- Source coordinates are estimated with the 295 ICRF2 datum sources being used to define the frame. Note that this is different for the ICRF3 where a new set of 303 sources is used to define the frame.

As mentioned before, in one of the two solutions the GA is corrected, in the other it is not. This is the only difference between these solutions.

4 Results and Discussion

When the Vector Spherical Harmonic (VSH) decomposition is performed on the difference vector field of the two solutions, the parameters listed in Table 1 are found. The formal errors of the VSH parameters are generally lower than 0.1 μas. Looking at Table 1 one can immediately see the parameters most affected by GA which are the D_2 and D_3 parameters.

The apparent proper motion field, which can be expected from GA, resembles a flow from a source (galactic anti-center) to a sink (Galactic Center). In the VSH, the glide parameters describe a similar dipole pattern with a flow from a source to a diametrically opposed sink. The D_2 parameter describes a dipole with the poles at 18^{h} (note that this is almost exactly the same right ascension as the Galactic Center) and 6^{h} in right ascension and zero in declination, while the D_3 parameter describes a dipole with poles at $\pm 90^{\circ}$ declination and zero right ascension. Therefore, a combination of D_2 and D_3 is sufficient to describe most of the effect of GA.

Other parameters do show a small (couple of μas) variation as well. However, when looking at the correlation between the parameters, it can be seen that some of these parameters are correlated with factors as high as 0.46, see Table 3. This is most likely the reason for the other small parameters. One explanation for the correlations is the uneven distribution of the sources on the celestial sphere.

We can calculate the amplitude and direction of the glide (D_1, D_2, and D_3 parameters). This is listed in Table 2. One can see that the estimated direction is very close to the anti-center of the Galaxy.

This becomes even more evident when the glide is plotted on the celestial sphere, see Figure 1. One can see that the direction of the glide points almost exactly to the center of the Milky Way.

5 Conclusions

We created two CRF solutions with parameterization close to ICRF3 with the difference that in one of those solutions the effect of galacto-centric acceleration is corrected. Using a vector spherical harmonic decomposition of the difference vector field of these solutions we can show that correcting GA affects the glide parameters. In particular, the D_2 and D_3 parameters are affected by GA with a difference of 30 μas and 15 μas,

Table 1 VHS parameters of degree 2 between the Vienna CRF solution with correction of GA and without correction of GA.

	[μas]
R_1	-6 ± 0.1
R_2	$+3 \pm 0.1$
R_3	-3 ± 0.0
D_1	$+2 \pm 0.1$
D_2	$+31 \pm 0.1$
D_3	$+15 \pm 0.1$
$a^{e}_{2,0}$	$+4 \pm 0.1$
$a^{m}_{2,0}$	$+0 \pm 0.1$
$a^{e,Re}_{2,1}$	-0 ± 0.1
$a^{e,Im}_{2,1}$	$+2 \pm 0.1$
$a^{m,Re}_{2,1}$	-2 ± 0.1
$a^{m,Im}_{2,1}$	$+0 \pm 0.1$
$a^{e,Re}_{2,2}$	-0 ± 0.0
$a^{e,Im}_{2,2}$	$+0 \pm 0.0$
$a^{m,Re}_{2,2}$	$+0 \pm 0.0$
$a^{m,Im}_{2,2}$	$+0 \pm 0.0$

Table 2 Amplitude and direction of glide between the Vienna CRF solution with correction of GA and without correction of GA.

	[μas]
Glide Amplitude	$+35 \pm 0.1$
Glide RA	$+86 \pm 0.1$
Glide DEC	$+25 \pm 0.1$

Table 3 Correlation of VSH parameters between the Vienna CRF solution with correction of GA and without correction of GA. To improve readability the correlations between the quadrupole parameters are omitted. The largest correlation between quadrupole parameters is -0.25.

	R_1	R_2	R_3	D_1	D_2	D_3
R_2	$+0.12$					
R_3	-0.13	-0.16				
D_1	$+0.03$	$+0.43$	-0.07			
D_2	-0.46	-0.03	$+0.04$	-0.07		
D_3	$+0.01$	-0.02	$+0.01$	$+0.03$	$+0.08$	
$a^{e}_{2,0}$	$+0.01$	$+0.02$	$+0.00$	-0.03	-0.00	-0.36
$a^{m}_{2,0}$	-0.03	-0.07	$+0.33$	-0.17	$+0.14$	$+0.00$
$a^{e,Re}_{2,1}$	-0.00	$+0.02$	$+0.01$	$+0.32$	$+0.04$	$+0.01$
$a^{e,Im}_{2,1}$	$+0.06$	-0.02	$+0.00$	-0.03	-0.37	-0.01
$a^{m,Re}_{2,1}$	-0.40	-0.03	$+0.04$	-0.08	$+0.29$	-0.07
$a^{m,Im}_{2,1}$	$+0.04$	$+0.37$	-0.05	$+0.40$	-0.08	-0.08
$a^{e,Re}_{2,2}$	$+0.02$	-0.03	-0.00	-0.02	$+0.01$	$+0.04$
$a^{e,Im}_{2,2}$	$+0.02$	$+0.01$	$+0.02$	$+0.07$	$+0.03$	$+0.05$
$a^{m,Re}_{2,2}$	-0.02	-0.01	-0.02	-0.08	-0.07	-0.15
$a^{m,Im}_{2,2}$	-0.02	-0.03	-0.03	-0.09	$+0.08$	$+0.15$

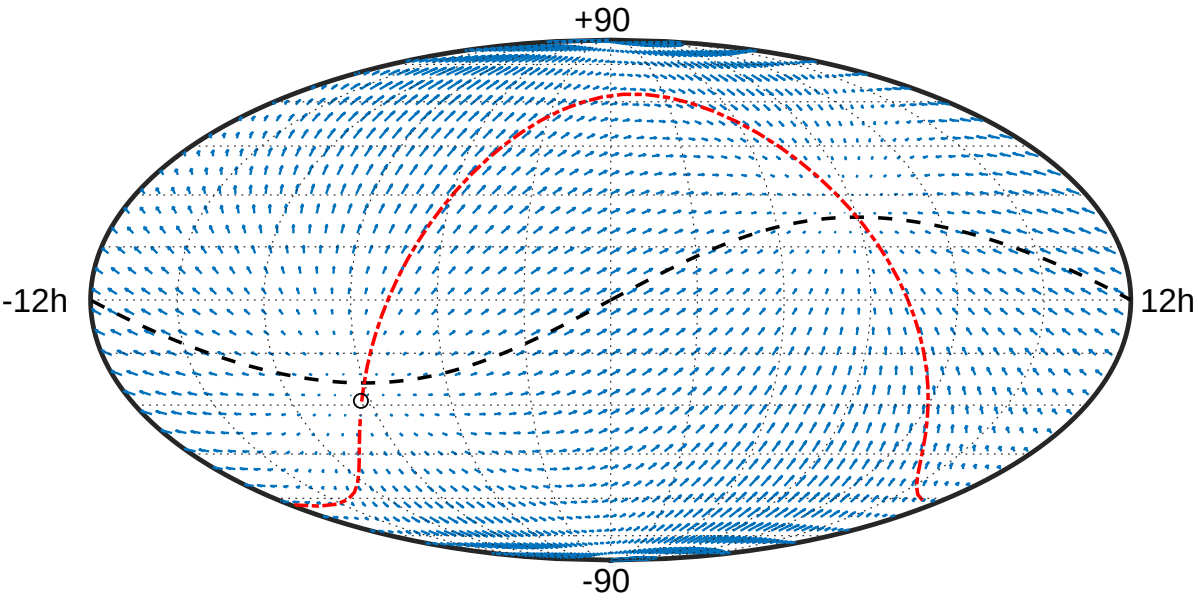

Fig. 1 Glide between the Vienna CRF solution with correction of GA and without correction of GA. The largest arrow has a size of 35 µas. The ecliptic is plotted in black and the galactic plane is plotted in red. The center of the galaxy is denoted as a black circle.

respectively. Other parameters show a small dependence of a couple of µas. However, since correlations of up to 0.46 between the parameters exist these small transformation parameters are most likely not a real effect.

References

1. Altamimi, Z., Rebischung, P., Métivier, L. and Collilieux, X. ITRF2014: A new release of the international terrestrial reference frame modeling nonlinear station motions. *Journal of Geophysical Research: Solid Earth*, 121(8), 6109–6131, 2016. http://dx.doi.org/10.1002/2016JB013098
2. Böhm, J., Werl, B. and Schuh, H. Troposphere mapping functions for GPS and very long baseline interferometry from european centre for medium-range weather forecasts operational analysis data. *Journal of Geophysical Research: Solid Earth*, 111 (B2), 2006. http://dx.doi.org/10.1029/2005JB003629
3. Böhm, J. et al. Vienna VLBI and Satellite Software (VieVS) for Geodesy and Astrometry. *Publications of the Astronomical Society of the Pacific*, 130(986), 2018. http://stacks.iop.org/1538-3873/130/i=986/a=044503
4. Charlot, P. et al. The Third Realization of the International Celestial Reference Frame by Very Long Baseline Interferometry. *A&A*, to be submitted, 2018.
5. Fey, A. L. et al. The Second Realization of the International Celestial Reference Frame by Very Long Baseline Interferometry. *The Astronomical Journal*, 150(2), 58, 2015. http://stacks.iop.org/1538-3881/150/i=2/a=58
6. Ma, C. et al. The Second Realization of the International Celestial Reference Frame by Very Long Baseline Interferometry. *IERS Technical Note 35*, 2009. https://www.iers.org/IERS/EN/Publications/TechnicalNotes/tn35.html
7. MacMillan, D. S. Atmospheric gradients from very long baseline interferometry observations. *Geophysical Research Letters*, 22(9), 1041–1044, 1995. http://dx.doi.org/10.1029/95GL00887
8. MacMillan, D. S. and Ma, C. Atmospheric gradients and the VLBI terrestrial and celestial reference frames. *Geophysical Research Letters*, 24(4), 453–456, 1997. http://dx.doi.org/10.1029/97GL00143
9. MacMillan, D. S. et al. Final Report of the IVS Working Group 8 (WG8) on Galactic Aberration, 2018.
10. Mignard, F. and Klioner, S. Analysis of astrometric catalogues with vector spherical harmonics. *A&A*, 547, A59, 2012. https://doi.org/10.1051/0004-6361/201219927
11. Petit, G. and Luzum, B., eds. IERS Technical Note No. 36. *IERS Conventions 2010*, Frankfurt am Main: Verlag des Bundesamts für Kartographie und Geodäsie, 2010. http://iers-conventions.obspm.fr/updates/2010updatesinfo.php
12. Titov, O., Lambert, S. B. and Gontier, A.-M. VLBI measurement of the secular aberration drift. *A&A*, 529, A91, 2011. https://doi.org/10.1051/0004-6361/201015718
13. Titov, O. and Lambert, S. Improved vlbi measurement of the solar system acceleration. *A&A*, 559, A95,2013. https://doi.org/10.1051/0004-6361/201321806

14. Titov, O. and Krásná, H. Measurement of the solar system acceleration using the earth scale factor. *A&A*, 610, A36, 2018. https://doi.org/10.1051/0004-6361/201731901
15. Wijaya, D., Böhm, J., Karbon, M., Krásná, H. and Schuh, H. Atmospheric Pressure Loading. *Atmospheric Effects in Space Geodesy*, Springer Berlin Heidelberg, Berlin, Heidelberg, pp. 137–157, 2013 http://dx.doi.org/10.1007/978-3-642-36932-2_4
16. Xu, M. H., Wang, G. L. and Zhao, M. The solar acceleration obtained by VLBI observations *A&A*, 544, A135, 2012. https://doi.org/10.1051/0004-6361/201219593